

Tomographic image alignment in three-dimensional coherent diffraction microscopy

Chien-Chun Chen,¹ Jianwei Miao,² and T. K. Lee¹¹*Institute of Physics, Academia Sinica, Nankang, Taipei 11529, Taiwan*²*Department of Physics and Astronomy and California NanoSystems Institute, University of California–Los Angeles, Los Angeles, California 90095, USA*

(Received 18 November 2008; published 27 February 2009)

We report the development of a tomographic image alignment method, based on the moment of charge density, for three-dimensional (3D) coherent diffraction microscopy. By using a 3D model system, we demonstrate that the moment of charge density improves the alignment accuracy over the conventional cross-correlation method. Better results are also obtained when we apply this method to the alignment of 27 experimental projections from a GaN-Ga₂O₃ quantum dot nanoparticle.

DOI: 10.1103/PhysRevB.79.052102

PACS number(s): 42.30.Wb, 61.05.cp, 68.37.Yz

Coherent diffraction microscopy is a lensless imaging technique in which the coherent diffraction pattern of a non-crystalline specimen is measured and then directly phased by the oversampling phasing algorithm.¹ Since its first experimental demonstration in 1999,² coherent diffraction microscopy has been successfully applied to imaging of a variety of samples, ranging from nanoparticles, nanocrystals, biomaterials, whole cells, and single viruses to carbon nanotubes by using x rays, electrons, high-harmonic generation sources, and soft x-ray lasers.^{3–22} An important direction of coherent diffraction microscopy is to perform quantitative three-dimensional (3D) imaging of materials and biological specimens at high resolutions. Currently, there are two schemes for obtaining 3D structural information by coherent diffraction imaging. One is based on direct phase retrieval of a 3D diffraction pattern interpolated from a limited number of two-dimensional (2D) patterns.^{4,20–22} However, since the diffraction intensity varies at least 5–7 orders from high to low resolution, reciprocal-space interpolation unavoidably introduces artifacts in the assembled 3D diffraction pattern and the reconstructed 3D image. The problem may become more severe for the characterization of 3D structures at the nanometer resolution where fewer data points at higher spatial frequency are available for interpolation. The other scheme is implemented through the combination of (i) *ab initio* phase retrieval of 2D coherent diffraction patterns with iterative algorithms^{7,23,24} and (ii) 3D tomographic image reconstruction.¹² The difficulty in this scheme is the requirement of aligning the 2D projection images to a common rotation axis for 3D reconstruction.

To solve this alignment problem, the “cross-correlation” method (CCM) used in electron tomography works well when successive projections are taken with a small angular increment.^{25,26} However, for the x-ray-diffraction measurements, the number of projections is sometimes limited due to, e.g., radiation damage to biological specimens,²⁷ which makes the CCM method less reliable. In addition, CCM also accumulates alignment errors by comparing the projection images reconstructed from consecutive angles. In this Brief Report, we present a method for precise alignment of 2D projection images. The 3D reconstruction of the aligned 2D projections are performed by using equally sloped tomography (EST), in which the projections are acquired at an equal slope increment.²⁸ It has been shown in computer simula-

tions and experiments that when the number of projections is limited, the EST reconstruction is superior to the conventional tomographic methods based on equally angled projections.^{28,29}

The image alignment method is based on the concept of moment of charge density distribution, defined as

$$R = \sum_i r_i \rho(r_i) / \sum_j \rho(r_j), \quad (1)$$

where R is the moment of charge density, and $\rho(r_i)$ and $\rho(r_j)$ are the electron densities of a projection image at positions i and j . By using Eq. (1), we calculate the moments of charge density along the X and Y axes, $X(\theta)$ and $Y(\theta)$, for the 2D projection images at different θ . Here the specimen is assumed to be tilted around a common rotation axis (the Y axis) and the beam direction is along the Z axis. Since Y is the rotation axis, $Y(\theta)$ should be the same for all projection images, which can be used to align all projections along the Y axis. A simple approach is to select the projection at 0° to be the reference projection and shift the other projections to match $Y(0)$.

After the alignment of all the projections along the Y axis, we choose a reference coordinate system with the origin at the center of the Y axis. Based on this reference coordinate system, the moment of charge density for an aligned projection at a specific angle is a linear combination of the X and Z

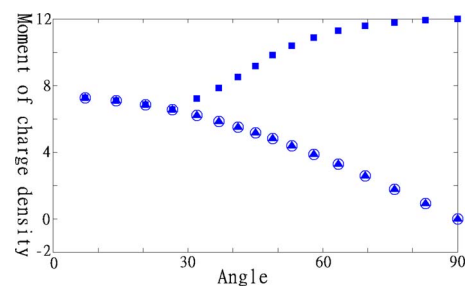


FIG. 1. (Color online) The moment of charge density, calculated from 32 projections, as a function of the angle. Triangles and squares are the results from our method and CCM, respectively. Triangles coincide with the circles, which are the exact results of the model.

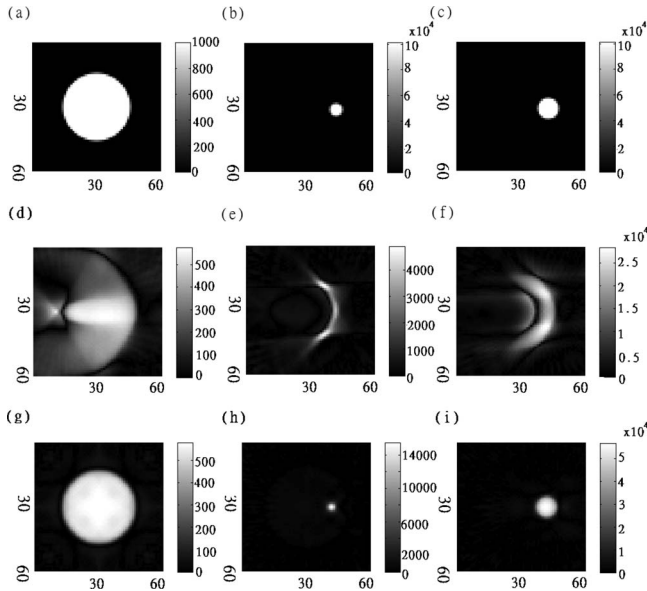


FIG. 2. Comparison of the tomographic reconstructions of a 3D model system from 32 projections aligned by CCM and the moment of charge density method. [(a)–(c)] Original three slices of the 3D model at 95–105, 145–155, and 195–205 nm, respectively. [(d)–(f)] Three corresponding slices of the reconstructed model from 32 projections by using the CCM alignment. [(g)–(i)] Three corresponding slices of the reconstructed model from 32 projections by using the moment of charge density alignment method. The grayscale represents the density distribution and the indices on the left and below the panels are the pixel numbers.

components of the moment of the charge density at other angles, e.g.,

$$X_a(45 + \theta) = X_a(45)\cos(\theta) - Z_a(45)\sin(\theta), \quad (2)$$

where the subscript a represents the reference coordinate system with all the projections aligned, and the equation is

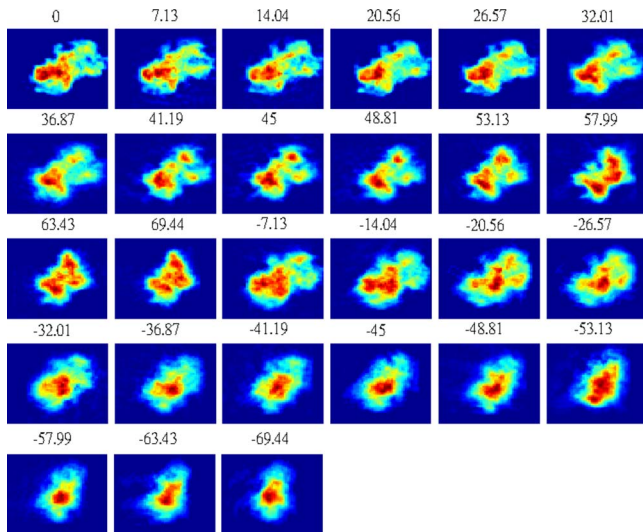


FIG. 3. (Color online) 27 reconstructed images of a GaN-Ga₂O₃ quantum dot nanoparticle, aligned by the moment of charge density method. Each angle is shown on the top of panel (in degrees).

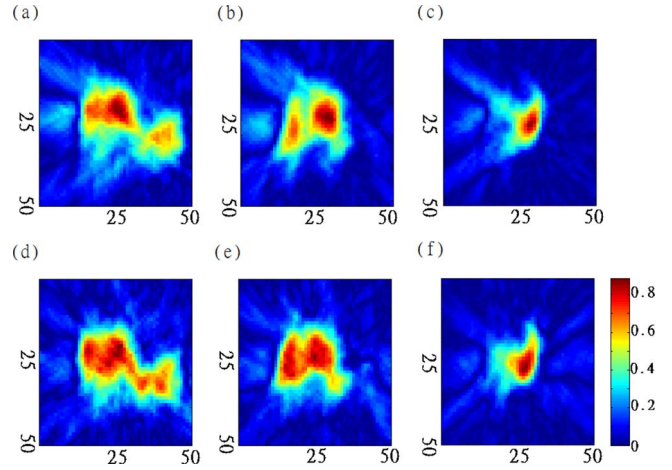


FIG. 4. (Color online) Three slices of the 3D reconstructed GaN-Ga₂O₃ structure at 153–170, 238–255, and 323–340 nm, respectively. [(a)–(c)] Three corresponding slices reconstructed from 27 projections aligned by CCM. [(d)–(f)] Three corresponding slices through the moment of charge density alignment method. The color represents the density distribution and the indices on the left and below the panels are the pixel numbers.

obtained by using matrix rotation. Since the projection images are reconstructed from the diffraction patterns alone, shifting of the projection along the X and Y axes is indistinguishable for the phase retrieval algorithms. Hence we have $X(\theta) = X_a(\theta) + d(\theta)$, where $d(\theta)$ represents the shifted distance along the X axis and is an integral number of pixels. This is because the smallest phase shift in the phase retrieval algorithms based on the fast Fourier transform is determined by a pixel. Applying Eq. (2) to $45^\circ + \theta$ and $45^\circ - \theta$, we obtain

$$\begin{aligned} X(45 + \theta) + X(45 - \theta) - 2[X(45) - d(45)]\cos(\theta) \\ = d(45 + \theta) + d(45 - \theta). \end{aligned} \quad (3)$$

For a specific θ , we calculate $X(45 + \theta)$, $X(45 - \theta)$, and $X(45)$ by using Eq. (1). The unknown variables in Eq. (3) are $d(45)$, $d(45 + \theta)$, and $d(45 - \theta)$ which are nevertheless integers. We determine $d(45)$ by making $d(45 + \theta) + d(45 - \theta)$ an integer. Once we know $d(45)$, then $X_a(45)$ is obtained. By using the same strategy, we calculate $X_a(-45)$. It is obvious from Eq. (2) that $Z_a(45)$ is equal to $X_a(-45)$ when $\theta = -90^\circ$. Once $Z_a(45)$ and $X_a(45)$ are known, the moment of charge density of the other angles can be calculated for the reference coordinate system based on Eq. (2). After obtaining $X_a(\theta)$ at each angle, we shift the $X(\theta)$ to match $X_a(\theta)$ and hence all the projections are aligned. A special advantage of the moment of charge density is that it allows double checking of the alignment errors by using other angles. There are a number of angles we may use because the diffraction patterns are acquired at an equally sloped increment; i.e., it is symmetrical around 45° and -45° .^{28,29}

To quantitatively compare the moment of charge density method with CCM, we constructed a 3D model which has a big ball with a diameter of 400 nm and an inner small ball with a diameter of 100 nm. The electron density of the small ball is 100 times larger than that of the big one. The center of

TABLE I. The error functions defined by Eq. (5) are listed for all the angles. The columns from left to right are error functions of 3D reconstructed object through CCM and the moment alignment method.

Angle (deg)	CCM	Our method
0	0.371	0.340
7.13	0.354	0.323
14.04	0.342	0.310
20.56	0.331	0.300
26.57	0.323	0.295
32.01	0.325	0.299
36.87	0.352	0.337
41.19	0.350	0.337
45	0.361	0.329
48.81	0.362	0.327
53.13	0.351	0.317
57.99	0.361	0.309
63.43	0.353	0.295
69.44	0.434	0.369
-7.13	0.381	0.356
-14.04	0.379	0.372
-20.56	0.375	0.370
-26.57	0.369	0.340
-32.01	0.385	0.341
-36.87	0.378	0.352
-41.19	0.393	0.371
-45	0.409	0.361
-48.81	0.409	0.348
-53.13	0.383	0.340
-57.99	0.346	0.297
-63.43	0.353	0.332
-69.44	0.423	0.381
Average	0.368	0.335

big ball is at the origin and the center of the small one is 120 nm apart from the origin along the X axis. We also set the beam direction along the Z axis and the rotation axis along the Y axis. In the simulation, 32 equally sloped projections were distributed from -90° to 90° with the pixel size of 10 nm.

We randomly shifted the 32 projections by a few pixels along the X and Y axes and then aligned them by using our method and CCM. Figure 1 shows the moment of charge density of the 32 projections along the X axis as a function of the angle. The triangles represent the moments of charge density obtained by our method which coincide with the exact results of the model (circles). The squares represent the data points obtained by CCM where we used a simple version of CCM. To align two projection images ρ_1 and ρ_2 , we shifted ρ_2 to have the maximum value of cross correlation at $r=0$. The cross correlation $\rho_1(r) * \rho_2(r)$ is calculated by

$$\rho_1(r) * \rho_2(r) = \int_{-\infty}^{\infty} \rho_1(r') \rho_2(r+r') dr'. \quad (4)$$

Figure 1 shows that the CCM works well below 30° . But for larger angles CCM misaligned the position of the moment of charge density along the X axis. Using the cross correlation as a criterion, CCM tends to align two consecutive projections by maximizing their overlap, which may deviate from the correct solution when the angular increment of the projections is relatively large. Another problem with CCM is the accumulation of alignment errors. Since it is based on the cross correlation of successive projections, an alignment error in one angle will be carried on to the next angle. As shown in Fig. 1, the position of the moment of charge density differs from the exact one after 32° . The difference increases linearly until it reaches 90° with an error of 12 pixels.

Figures 2(a)–2(c) show three slices of the model at 95–105, 145–155, and 195–205 nm of the model, respectively. Figures 2(d)–2(f) show the same three slices of the reconstructed model from 32 projections, aligned by CCM. The 3D tomographic reconstruction was performed by using the EST method.^{28,29} The misalignment of the projections between 32° and 90° by CCM causes significant distortion in the reconstructed image. Figures 2(g)–2(i) show the same three slices of the reconstructed model by using the moment of charge density alignment method, which are almost identical to the original slices except for some weak streaks outside the sphere. These streaks are caused by the 3D tomographic reconstruction from a limited number of projections.

We have also applied the moment of charge density method to the 3D image reconstruction of a GaN-Ga₂O₃ quantum dot nanoparticle. By using an undulator beamline at SPring-8, we obtained a tilt series of 27 coherent x-ray-diffraction patterns from a single micron-sized GaN-Ga₂O₃ nanoparticle.³⁰ The diffraction patterns were directly inverted to 2D images by the guided hybrid input-output algorithm.²⁴ Using the moment of charge density method, we aligned the 27 reconstructed images, shown in Fig. 3. The consistency of the alignment was verified by using a few pairs of angles. For a comparison purpose, we also aligned the 27 images by CCM. The 3D tomographic reconstruction was performed by EST. Figure 4 shows three slices of the 3D reconstructed image at 153–170, 238–255, and 323–340 nm, respectively, where the upper panel [(a)–(c)] was obtained by CCM and the lower panel [(d)–(f)] was obtained by the moment of charge density. Careful examination of Fig. 4 indicates that the 3D reconstruction through CCM is more distorted and discontinuous than that through the moment of charge density alignment method. The streaks in Figs. 4(d)–4(f) are due to the tomographic reconstruction from a limited number of projections.

The improvement of the moment alignment method could be further demonstrated by comparing the diffraction amplitudes between the reconstructed object and experimental data directly. Define the error function as

$$\text{erf} = \frac{\sum_{k \in D} ||H(k)| - |F(k)||}{\sum_{k \in D} |F(k)|}, \quad (5)$$

where $|H(k)|$ and $|F(k)|$ are the Fourier amplitudes of reconstructed image and experimental amplitudes, respectively. The range of diffraction pattern, D , is chosen for the central 401×401 pixels with high signal-to-noise ratio. Table I lists the calculated error functions at all angles. The moment alignment method has reduced 10%–20% errors of the result of CCM method.

In summary, we developed the moment of charge density method to resolve the image alignment problem in 3D coherent diffraction microscopy. By using a 3D model system, we demonstrated that the method improves the alignment accuracy over the commonly used CCM approach.^{25,26} CCM tends to produce large errors when the projections are taken with a large angular increment, and also accumulates align-

ment errors from successive projections. Furthermore, it is difficult to double check the alignment accuracy obtained by CCM. All of these difficulties are resolved by using the moment of the charge density for alignment target. We applied this method to the 3D reconstruction of a GaN-Ga₂O₃ quantum dot particle from 27 coherent x-ray-diffraction patterns. The 3D structure obtained by the moment of charge density method indeed improved over that obtained by CCM. We believe that this alignment method not only can be used for 3D coherent diffraction microscopy, but also may be applicable to other tomographic reconstructions.

We thank C. Song, Y. Nishino, and Y. Kohmura for data acquisition and data analysis of the GaN-Ga₂O₃ nanoparticle and S. Risbud for providing the sample. This work was supported in part by the U.S. DOE, BES (Grant No. DE-FG02-06ER46276), and the U.S. NSF (Grant No. DMR-0520894). Use of the RIKEN beamline (BL29XUL) at SPring-8 was supported by RIKEN.

-
- ¹J. Miao, T. Ishikawa, T. Earnest, and Qun Shen, *Annu. Rev. Phys. Chem.* **59**, 387 (2008).
- ²J. Miao, P. Charalambous, J. Kirz, and D. Sayre, *Nature (London)* **400**, 342 (1999).
- ³I. K. Robinson, I. A. Vartanyants, G. J. Williams, M. A. Pfeifer, and J. A. Pitney, *Phys. Rev. Lett.* **87**, 195505 (2001).
- ⁴J. Miao, T. Ishikawa, B. Johnson, E. H. Anderson, B. Lai, and K. O. Hodgson, *Phys. Rev. Lett.* **89**, 088303 (2002).
- ⁵J. M. Zuo, I. Vartanyants, M. Gao, R. Zhang, and L. A. Nagahara, *Science* **300**, 1419 (2003).
- ⁶J. Miao, K. O. Hodgson, T. Ishikawa, C. A. Larabell, M. A. LeGros, and Y. Nishino, *Proc. Natl. Acad. Sci. U.S.A.* **100**, 110 (2003).
- ⁷S. Marchesini, H. He, H. N. Chapman, S. P. Hau-Riege, A. Noy, M. R. Howells, U. Weierstall, and J. C. H. Spence, *Phys. Rev. B* **68**, 140101(R) (2003).
- ⁸D. Shapiro, P. Thibault, T. Beetz, V. Elser, M. Howells, C. Jacobsen, J. Kirz, E. Lima, H. Miao, A. M. Neiman, and D. Sayre, *Proc. Natl. Acad. Sci. U.S.A.* **102**, 15343 (2005).
- ⁹M. A. Pfeifer, G. J. Williams, I. A. Vartanyants, R. Harder, and I. K. Robinson, *Nature (London)* **442**, 63 (2006).
- ¹⁰H. M. Quiney, A. G. Peele, Z. Cai, D. Paterson, and K. A. Nugent, *Nat. Phys.* **2**, 101 (2006).
- ¹¹H. N. Chapman *et al.*, *Nat. Phys.* **2**, 839 (2006).
- ¹²J. Miao, C. C. Chen, C. Song, Y. Nishino, Y. Kohmura, T. Ishikawa, D. Ramunno-Johnson, T. K. Lee, and S. H. Risbud, *Phys. Rev. Lett.* **97**, 215503 (2006).
- ¹³G. J. Williams, H. M. Quiney, B. B. Dhal, C. Q. Tran, K. A. Nugent, A. G. Peele, D. Paterson, and M. D. de Jonge, *Phys. Rev. Lett.* **97**, 025506 (2006).
- ¹⁴J. M. Rodenburg, A. C. Hurst, A. G. Cullis, B. R. Dobson, F. Pfeiffer, O. Bunk, C. David, K. Jefimovs, and I. Johnson, *Phys. Rev. Lett.* **98**, 034801 (2007).
- ¹⁵R. L. Sandberg, A. Paul, D. A. Raymondson, S. Hadrich, D. M. Gaudiosi, J. Holtsnider, R. I. Tobey, O. Cohen, M. M. Murnane, H. C. Kapteyn, C. Song, J. Miao, Y. Liu, and F. Salmassi, *Phys. Rev. Lett.* **99**, 098103 (2007).
- ¹⁶R. L. Sandberg, C. Song, P. W. Wachulak, D. A. Raymondson, A. Paul, B. Amirbekian, E. Lee, A. E. Sakdinawat, M. C. Marconi, C. S. Menomi, M. M. Murnane, J. J. Rocca, H. C. Kapteyn, and J. Miao, *Proc. Natl. Acad. Sci. U.S.A.* **105**, 24 (2008).
- ¹⁷H. Jiang, D. Ramunno-Johnson, C. Song, B. Amirbekian, Y. Kohmura, Y. Nishino, Y. Takahashi, T. Ishikawa, and J. Miao, *Phys. Rev. Lett.* **100**, 038103 (2008).
- ¹⁸C. Song, H. Jiang, A. Mancuso, B. Amirbekian, L. Peng, R. Sun, S. S. Shah, Z. H. Zhou, T. Ishikawa, and J. Miao, *Phys. Rev. Lett.* **101**, 158101 (2008).
- ¹⁹P. Thibault, M. Dierolf, A. Menzel, O. Bunk, C. David, and F. Pfeiffer, *Science* **321**, 379 (2008).
- ²⁰A. Barty *et al.*, *Phys. Rev. Lett.* **101**, 055501 (2008).
- ²¹H. N. Chapman *et al.*, *J. Opt. Soc. Am. A Opt. Image Sci. Vis.* **23**, 1179 (2006).
- ²²Y. Takahashi, Y. Nishino, T. Ishikawa, and E. Matsubara, *Appl. Phys. Lett.* **90**, 184105 (2007).
- ²³J. R. Fienup, *Appl. Opt.* **21**, 2758 (1982).
- ²⁴C. C. Chen, J. Miao, C. W. Wang, and T. K. Lee, *Phys. Rev. B* **76**, 064113 (2007).
- ²⁵W. O. Saxton and J. Frank, *Ultramicroscopy* **2**, 219 (1976).
- ²⁶R. Guckenberger, *Ultramicroscopy* **9**, 167 (1982).
- ²⁷J. Kirz, C. Jacobsen, and M. Howells, *Q. Rev. Biophys.* **28**, 33 (1995).
- ²⁸J. Miao, F. Forster, and O. Levi, *Phys. Rev. B* **72**, 052103 (2005).
- ²⁹E. Lee, B. P. Fahimian, C. V. Iancu, C. Suloway, G. E. Murphy, E. R. Wright, D. Castano-Diez, G. J. Jensen, and J. Miao, *J. Struct. Biol.* **164**, 221 (2008).
- ³⁰J. Miao, Y. Nishino, Y. Kohmura, B. Johnson, C. Song, S. H. Risbud, and T. Ishikawa, *Phys. Rev. Lett.* **95**, 085503 (2005).